Food Chemistry: X 24 (2024) 101930

Contents lists available at ScienceDirect

Food Chemistry: X

journal homepage: www.sciencedirect.com/journal/food-chemistry-x

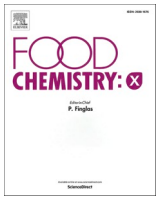

Intelligent color changing packaging film based on esterified starch and black rice anthocyanins

Wei Song [a], Nan Wu [b], Yikai He [b], Huaixiang Zhao [a], Jian Xu [b], Lili Ren [b,*]

[a] College of Engineering and Technology, Jilin Agricultural University, Changchun 130118, China
[b] Key Laboratory of Bionic Engineering (Ministry of Education), College of Biological and Agricultural Engineering, Jilin University, Changchun 130022, China

ARTICLE INFO

Keywords:
Intelligent packaging
Black rice anthocyanins
Starch-based film
Mechanical properties
Esterified starch

ABSTRACT

Intelligent packaging film has received more and more attention because it can help consumers obtain more intuitive information about the packaging, provide better preservation and advanced convenience. In this study, black rice anthocyanin (BRA) was added into composite film formed by starch (S) and esterified starch (ES). As the BRA content increased, the thickness and the total color difference of the S/ES-BRA film increased. The opacity of S/ES-BRA film decreased relative to that of the film without BRA, but increased with the increase of anthocyanin. Compared with S/ES film, the elongation at break of S/ES-BRA0.5 film increased from 33.1 % to 45.4 %, and the tensile strength decreased from 7.3 to 5.8 MPa. S/ES-BRA film had response to different pH values and underwent color changes in different buffer solutions. Intelligent color changing packaging film will used to monitor food quality, water quality and soil properties.

1. Introduction

Food has a variety of forms such as solid, semi-solid and liquid, etc. For the packaging of food, plastic packaging can be found everywhere in life and has almost become an indispensable item. But non-biodegradable plastic packaging is a great burden on the environment, and will cause pollution of water and soil. Effective food packaging should not only be dust-proof and pollution-proof, but should also bring convenience to consumers in purchasing excellent quality food (Bangar et al., 2021; Dai et al., 2019). Typically, customers check and confirm the quality of a food product by looking at the date of manufacture and shelf life displayed on the package, but for foods that are perishable, it is critical to be able to monitor quality in real time (Hasanah et al., 2023). Intelligent food packaging film could monitor food quality in real time by sensing pH, temperature, humidity, light, and gas evaporation during the food spoilage process. In order to make food products available to meet the needs of customers, biodegradable intelligent packaging has started to replace the previous plastic packaging with biodegradable intelligent packaging. Therefore, it is urgent to find an economical, green, safe and intelligent packaging material.

In fact, intelligent packaging is a trend in food packaging in recent years. Plant extracts, essential oils, cross-linking agents, and nano-materials are used in packaging to improve the mechanical and physical properties of the film (Kumar et al., 2023). Starch is widely available in nature, abundant, easily accessible and inexpensive. It is because starch also inherits these advantages when mixed with other materials that it plays an important role in intelligent packaging. Starch as a universal substrate material, after gelatinization, films are combined to form the hydroxyl groups between the starch through the in-termolecular hydrogen bonding easily. Therefore, they are often used as films or coatings in intelligent packaging to improve the quality of food and extend its storage time (Cui et al., 2021; Hu et al., 2019). Starch-based films are biodegradable, renewable, edible, have high transparency, bio-compatibility and low odor, and have been used to package a wide range of food products. However, starch-based packaging films are not widely used in the packaging industry, mainly because of their poor mechanical, barrier and processing properties. Raw starch cannot be widely used in food packaging due to disadvantages such as hydrogen bonding, poor water resistance and solubility. To overcome these drawbacks, they can be modified or blended with other materials. Esterified starch, as a type of modified starch, is added to the raw starch along with BRA to prepare a blend film, which is pH sensitive and has potential applications in the food packaging industry. These properties are influenced by the type of starch, temperature and time of film formation, etc. (Thakur et al., 2019). In order to overcome the drawbacks of starch, starch types with a higher content of straight-chain amylose are

* Corresponding author.
E-mail address: liliren@jlu.edu.cn (L. Ren).

https://doi.org/10.1016/j.fochx.2024.101930
Received 28 June 2024; Received in revised form 9 October 2024; Accepted 23 October 2024
Available online 24 October 2024
2590-1575/© 2024 The Authors. Published by Elsevier Ltd. This is an open access article under the CC BY-NC-ND license (http://creativecommons.org/licenses/by-nc-nd/4.0/).

generally used to improve the tensile strength of the film. However, higher content of straight chain starch can make the film more brittle. In addition, other functional materials such as antimicrobials, antioxidants, and inorganic carbon materials are usually added to the starch matrix to improve its performance. Selection of the right type of material in the right concentration can im-prove the properties of starch-based films. Natural starches are chemically modified to be used to improve the properties required to be suitable for use in films (Mehboob et al., 2020; Xu et al., 2022). Esterified starch, as a type of modified starch, plays an important role in improving the performance of starch-based packaging films. Compared with chitosan and polyvinyl alcohol, esterified starch is ageing resistant, lipophilic and has good emulsion stability. There is an ester bond in esterified starch, which also increases the hydrophobicity of the starch-based film since the ester group is a hydrophobic group (Amin et al., 2019). At the same time, the color of the film can be affected by the source of the starch and the method of modification, so esterified starch has great potential for starch-based intelligent packaging. However, few starch-based films have been prepared by blending esterified starch with starch.

There are many organisms in nature that accentuate their characteristics in their environment, for example, the chameleon's body color is a pale green when in water, and changes to brown in grass. Mimosas will quickly close their leaves in response to the slightest environmental vibration or irritation. Remarkably, they themselves can change in response to changes in the environment and are used to protect themselves from being killed. It is worth noting that the properties of intelligent packaging materials can also be analyzed in intelligent packaging by changing the environment, e.g. light, temperature, pH, force, electricity and other stimuli. In terms of pH alone, anthocyanins are found in a wide variety of plants, fruits, vegetables and seeds from a wide range of sources but with complex extraction processes. The non-toxicity and safety of anthocyanins compared to synthetic pigments and dyes used in intelligent packaging has made it popular with researchers.

Anthocyanins are soluble in water, and in addition to their excellent properties as antioxidants, they are also capable of changing color with pH. Vedove et al. (Vedove et al., 2021) prepared pH indicator film using cassava starch and grape skin extract; Luchese et al. (Luchese et al., 2017) prepared intelligent packaging film using corn starch and blueberry powder, the mechanical properties of the films were improved by adding natural pigments to the starch. Adding anthocyanins to starch-based intelligent packaging can make the film pH-sensitive. Anthocyanins extracted from different plants show slightly different colors at the same pH value, which reflects the richness and diversity of anthocyanin colors (Bhargava et al., 2020). These properties make anthocyanins a great potential for intelligent packaging. In addition, anthocyanins have therapeutic effects on a number of systems in the human body, including the circulatory, nervous and immune systems. As a natural coloring agent, they may represent a chemical change in food products as they are pH-sensitive. Black rice anthocyanins prevent cardiovascular diseases, protect the liver, enhance vision, improve sleep, strengthen blood vessels, improve circulation, and remove harmful free radicals from the body, as well as effectively preventing cancer, which is highly beneficial to the human body. Therefore, it is more suitable for intelligent food packaging (Abedi-Firoozjah et al., 2022; Liu et al., 2021).

Anthocyanin stability is mainly affected by temperature, pH and initial concentration which in turn affects the packaging performance of the film material. Low pH and temperature favor anthocyanin stability in food products. It had been reported that anthocyanins would exist in the chalcone structure and the stability become very poor and the color was turned to colorless when the temperature rises to 60 °C (Grobelna et al., 2019). Black rice anthocyanins are heat-treated during the extraction step. The longer the heat treatment, the higher the initial concentration of extracted black rice anthocyanins, but they may be broken down more quickly during storage (Shernbagam et al., 2023).

In this paper, the composite films were prepared using starch, esterified starch and black rice anthocyanin as substrates. The films were characterized for thickness, swelling, transmittance, mechanical properties, FTIR, XRD, hygroscopicity, moisture permeability and pH sensitivity.

2. Materials and methods

2.1. Materials

Starch (S) and esterified starch (ES) were purchased from Changchun Jincheng Corn Development Co., Ltd., Da Cheng Group (Changchun, China). Corn starch with moisture content of 12.8 % and the amylose/amylopectin ratio of 28/72. Esterified starch (DS: 0.023) is modified with octenylsuccinic acid, under weak alkaline conditions, the reactive hydroxyl group on starch was replaced by a hydrophobic octenylsuccinic anhydride group to synthesise octenylsuccinic acid starch esters. Glycerol was supplied from Beijing Beihua Fine Chemicals Co., Ltd., (Beijing, China). Black rice anthocyanins (BRA, $C_{21}H_{21}O_{11}$, molecular weight: 449.38) was obtained from Xi'an Shengqing Biotechnology Co., Ltd., (Xi'an, China). All materials were used as received without further purification.

2.2. Preparation of S/ES-BRA films

Starch/esterified starch (S/ES) suspension was prepared by gelatinize starch (2.5 wt%) and esterified starch (2.5 wt%) in distilled water at 95 °C and stirring with 200 rpm for 60 min. Glycerin (30 wt% based on dry weight of starch and esterified starch) was added in suspension as a plasticizer. In order to maintain the function of anthocyanins and reduce the impact of environmental factors on their stability, during the process of adding anthocyanins to prepare the film, the temperature at 40–50 °C to ensure the chemical stability of anthocyanins. During food storage, high temperature or acidic or alkaline environments are also completely avoided. After starch/esterified starch suspension cooling down, a series of starch/esterified starch/black rice anthocyanin suspension was prepared by mixing S/ES starch suspension with BRA solution in the ratio 5:1 (*w*/w), stirring at 45 °C with 280 rpm for 30 min and denoted as S/ES-BRAx (x wt%: 0, 0.1, 0.3, 0.5 wt% based on the dry weight of starch and esterified starch). The /ES-BRA film suspension was cooled to room temperature for 20 min. The S/ES-BRA film suspension (pH value: 6.1) was cast on petri dishes and dried at 40 °C for 5 h. Temperatures above 50 °C begin to reduce preservation rates. During storage, the anthocyanin contents for all flower developmental stages were stable at pH 0.5–3.0, but the color of the extracts faded at higher pH values. After drying, S/ES-BRA0 films were stored at 75 % RH and S/ES-BRA0.1, 0.3 and 0.5 films were stored at 59 % RH in desiccators before further testing.

2.3. Scanning electron microscopy (SEM) of S/ES-BRA films

The cross-sections of S/ES-BRA film samples was visualized by using a scanning electron microscope (Zeiss Gemini SEM 360, Germany) operated at an accelerating voltage of 2 kV. Before measurement, the films were sputtered and coated with gold under vacuum.

2.4. FT-IR analysis of S/ES-BRA films

FT-IR spectra were measured by using a IRAffinity-1 Fourier Transform Infrared spectrophotometer (Shimadzu Corporation, Tokyo, Japan) to investigate the interactions of starch, esterified starch and BRA in the films. FT-IR spectra of S, ES and BRA powder and S/ES-BRA films were measured between 500 and 4000 cm^{-1} wavenumber range with a total of 64 scans.

2.5. Properties of S/ES-BRA films

2.5.1. Thickness of S/ES-BRA films

Thickness of S/ES-BRA films was measured by using a hand-held micrometer with a precision of 0.001 mm at five different positions in each S/ES-BRA film sample and the average values were taken. The thickness of S/ES-BRA films was used to calculate the density.

2.5.2. Color parameter of S/ES-BRA films

X-rite Ci64UV (USA) was used to determine the change of S/ES-BRA films color. The color values of L* (negative-dark; positive-light), a* (negative-green; positive-red) and b* (negative-blue; positive-yellow) were measured. A standard plate CX 2064 was used as standard. The color parameter values of the standard plate are L* = 94.52, a* = −0.86, and b* = 0.68. Five measurements were taken on each S/ES-BRA film sample. The total color difference (ΔE*) and color intensity (C*) were calculated as follows:

$$\Delta E^{*} = \sqrt{\Delta a^2 + \Delta b^2 + \Delta L^2} \tag{1}$$

$$C^{*} = \sqrt{a^2 + b^2} \tag{2}$$

where $\Delta L = L^{*}_{standard} - L^{*}_{sample}$, $\Delta a = a^{*}_{standard} - a^{*}_{sample}$, $\Delta b = b^{*}_{standard} - b^{*}_{sample}$.

2.5.3. Transparency of S/ES-BRA films

UV–vis spectra of S/ES-BRA films were performed using UV–Visible Spectrophotometer (Beijing Beifen Ruili Analytical Instrument Co., Ltd., Beijing, China). The analysis was performed by discontinuous scanning from 350 to 900 nm. Each film sample was cut into a rectangular piece and placed directly in a test cell and measurements were performed using unit as the reference. The opacity of S/ES-BRA films was calculated as follows:

$$Opacity = \frac{Abs}{d} \tag{3}$$

where Abs is the value of absorbance and d is the film thickness (mm).

2.6. Mechanical properties of S/ES-BRA films

S/ES-BRA films were cut into dumbbell-like samples with 50 mm length and 4 mm neck width. Mechanical properties of S/ES-BRA film samples were carried out by using a universal testing machine (Model LPS. 103C, MTS Systems Crop., USA) at a speed of 2 mm/min. Five samples were measured for each S/ES-BRA film and the average values were taken. The mechanical properties of S/ES-BRA films were calculated as follows:

$$Tensile\ strength\ (\mathrm{MPa}) = \frac{F}{d \times a} \tag{4}$$

$$Tensile\ strain\ (\%) = \frac{L_2 - L_1}{L_1} \times 100 \tag{5}$$

$$Young's\ modulus (GPa) = \frac{\sigma}{\varepsilon} \tag{6}$$

where F is the load of break (N), d is the thickness of S/ES-BRA film samples (mm), a is the width of S/ES-BRA film samples (mm), L_1 is the original length of S/ES-BRA film samples (mm), L_2 is the length of S/ES-BRA film samples (mm) at rupture.

2.7. X-ray diffraction spectra

X-ray diffraction (XRD) pattern of S/ES-BRA films and the ingredients of S/ES-BRA films was measured using a Lab XRD-3100 X-ray diffractometer (Shimadzu Corporation, Tokyo, Japan) with Cu radiation at 40 kV and 250 mA. The X-ray diffraction patterns were recorded at room temperature over the 2θ range of 3–50° at a speed of 2°/min. XRD data was processed in Jade software to analyze the crystallinity of the sample. The XRD data of the samples were entered in the software and before processing, the spectra of the samples were judged and observed for burrs and baseline shifts. The burrs in the spectra are removed by smoothing, then the baseline is levelled and finally the crystallinity of the sample is identified by reducing the fluctuations.

2.8. Water vapor permeability (WVP) of S/ES-BRA films

Water vapor permeability (WVP) tests were conducted gravimetrically according to the standard test method GB 1037–88 (similar to the relevant ASTM method). Special aluminum cups were used, which had 6.0 cm of internal diameter (exposed area: 28.26 cm^2) and 1.3 cm of depth. The aluminum cups were filled with anhydrous calcium chloride and fully dried at 200 °C for 2 h in order to provide 0 % relative humidity (RH) and sealed by S/ES-BRA film samples with wax. The aluminum cups and S/ES-BRA film samples were placed into a desiccator with 95 % RH at room temperature and weighed every 24 h. The WVP ($g \cdot m^{-1} \cdot s^{-1} \cdot Pa^{-1}$) of S/ES-BRA films was calculated as follows:

$$WVP = \frac{\Delta m \times d}{A \times t \times P \times (R_1 - R_2)} \tag{7}$$

where Δm (g) was the weight of water permeated through the film, d (m) was the thickness of the film, A (2.826×10^{-3} m^2) was the permeation area, t (h) was the time of permeation, and P (3179 Pa) is the saturation vapor pressure of water at the test temperature (22 °C), R_1 (%) is the relative humidity in the desiccator, R_2 (%) is the relative humidity inside the special aluminum cup.

2.9. Water absorption of S/ES-BRA films

S/ES-BRA films were cut into 20 mm × 20 mm samples and weighed (W_1) to measure the water absorption of S/ES-BRA films. The samples were immersed into water in a conical flask and shaken for 72 h at 45 °C, denoted as WA_{72h}. The S/ES-BRA films samples were then taken out and wiped water off surface to determine the final weight (W_2) of wet samples. The WS of S/ES-BRA films were calculated as follows:

$$Water\ absorption\ (\%) = \frac{W_2 - W_1}{W_1} \times 100\% \tag{8}$$

2.10. Moisture absorption of S/ES-BRA films

S/ES-BRA films were cut into 2 cm × 2 cm samples and dried at 45 °C for 12 h and weighed (W_1) to measure the moisture absorption of S/ES-BRA films. The S/ES-BRA film samples were then placed in desiccators with 5 different RH for 48 h and weighed (W_2). The moisture content (MC) of S/ES-BRA films was calculated as follows:

$$Moisture\ content\ (\%) = \frac{\mathrm{W_2 - W_1}}{\mathrm{W_1}} \times 100\% \tag{9}$$

2.11. The pH response of S/ES-BRA films

Different concentrations of buffer solution with pH ranged from 2 to 13 were prepared and recorded the color change of the film sample under different pH values. Film sample (1 cm × 1 cm) was immersed in different buffer solutions for 10 min. Then, the color changes of film sample were recorded by digital camera.

2.12. Application of pork belly monitoring

Fresh pork belly was acquired in local supermarket. A quantity of pork belly of the same freshness was transferred to 30 ml test bottle and

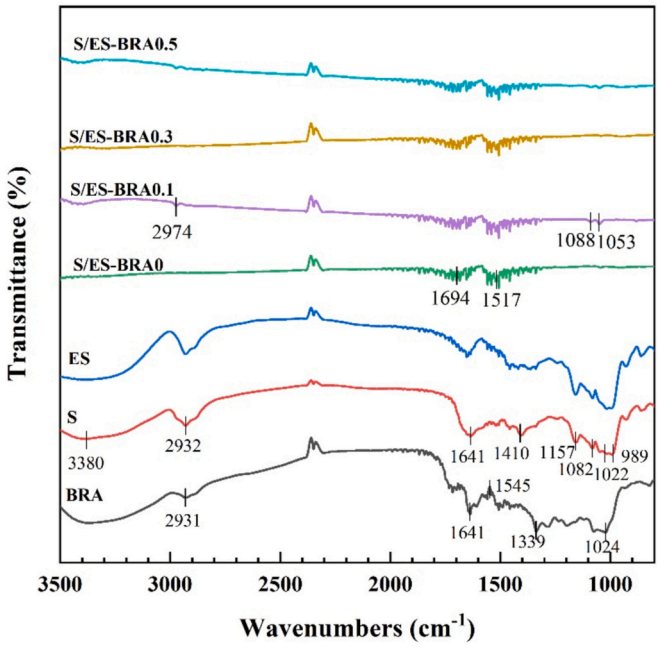

Fig. 1. FT-IR spectra for S, ES, BRA and S/ES-BRA films.

sealed with S/ES-BRA films. Unsealed test bottle was served as a control group throughout the testing process. The color of S/ES-BRA films was recorded at 0, 1, 3, 5 days at 4 °C.

2.13. Statistical analysis

The difference between factors and levels was evaluated by the analysis of variance (ANOVA). Duncan's multiple range tests were used to compare the means to identify which groups were significantly different from other groups ($p < 0.05$). All data are presented as mean ± standard deviation.

3. Results

3.1. FT-IR analysis of S/ES-BRA films

The FTIR spectra for S, ES, BRA and S/ES-BRA films are shown in Fig. 1. In the spectrum of S, the broad band appeared at 3370 cm^{-1} was due to hydrogen-bonded hydroxyl groups due to the stretching of –OH groups (Ren et al., 2017). The characteristic peak occurred at 2932 cm^{-1} was attributed to C—H stretches of hydrogen atoms from ring methine (Choi et al., 2017). The peak at 1641 cm^{-1} was due to the presence of O—H bending of bound water (Qin et al., 2020). C—H stretching of starch was observed at 1451 cm^{-1} (Zhang, Huang, et al., 2020). Bands at 1157 and 1082 cm^{-1} were attributed to bending and asymmetric stretching of C—O, C—C, and O—H bond stretching and C–O–C glycosidic bonds (Choi et al., 2017). The bands from 989 to 1022 cm^{-1} were assigned to the pyranose ring in the glucose residues of starch (Qin et al., 2020).

The spectrum of ES was similar to the spectrum of S, it did not reveal a new characteristic peak due to the spatial site resistance benefit and charge between the molecules and the low degree of substitution of the three hydroxyl groups of S.

The spectrum of BRA had a strong absorption band was presented at 1641 and 1545 cm^{-1}, corresponding to stretching vibrations of C═C aromatic rings (Choi et al., 2017). A series of absorption peaks from 1339 to 1024 cm^{-1} corresponded to the stretching vibration of C—O bonds in the glucosyl rings of the BRA (Zeng et al., 2023). After films formation, these bonds had shifted, these phenomena could be associated to the successful immobilization of anthocyanins into the starch (Huang et al., 2019).

Table 1
Density WVP and WA of S/ES-BRA film.

Film	Density ($g \cdot mm^{-3}$)	WVP ($\times 10^{-10}$ $g \cdot m^{-1} \cdot s^{-1} \cdot Pa^{-1}$)	WA_{72h} (wt%)
S/ES-BRA0	0.13 ± 0.00b	2.01 ± 0.23b	210.41 ± 1.43d
S/ES-BRA0.1	0.14 ± 0.00b	2.17 ± 0.20b	221.75 ± 1.26c
S/ES-BRA0.3	0.14 ± 0.00a	2.47 ± 0.17a	247.54 ± 1.99a
S/ES-BRA0.5	0.14 ± 0.01a	2.48 ± 0.13a	245.51 ± 1.59b

As can be seen in the spectrum of S/ES-BRA0 film, the mixture of S and ES caused the intensity of overall absorbance bands decreasing, this may be due to the breaking of hydrogen bonds that occurs during the gelatinize process. Compared with S/ES-BRA0 film, some differences in the position of peaks and the intensity of peak could be found after adding BRA. All S/ES-BRA films exhibited similar banding patterns with changes depending on the ingredients, which was due to the low content of BRA in the films. After the addition of BRA, the peaks of both S and ES starch were shifted or disappeared, indicating that starch and anthocyanins had formed intermolecular hydrogen bonds.

3.2. Physicochemical properties of S/ES-BRA films

The density of S/ES-BRA films was shown in Table 1. The density of S/ES-BRA films containing different concentrations of BRA had little difference and the density of S/ES-BRA films within BRA was greater than that of S/ES-BRA0 film because of the dispersion of BRA in the films making the structure more compact.

Color parameter is one of the important features of package films, especially in this study. Color can give feedback to the consumer visually about the condition of the product. Visually, the color of S/ES-BRA0 film was white and the color of S/ES-BRA film with BRA was pale purple which became darker as the concentration of BRA increasing from 0.1 to 0.5 wt%. The color parameters of S/ES-BRA films were shown in Fig. 2. As evident from the visual appearance and color parameters of S/ES-BRA films, after the addition of BRA, the L* value of S/ES-BRA film was decreased, the a* and b* values increased, which meant S/ES-BRA films became darker, redder and yellower. Compared with S/ES-BRA0 film (L* = 88.25, a* = 0.53, b* = −4.80), the L* value of S/ES-BRA0.5 film (78.85) decrease 9.40, the a* value (4.60) increased 4.07, the b* value (−0.65) increased 4.15. Consequently, the total color differences (ΔE*) of S/ES-BRA films gradually increased as the concentration of BRA increasing which was somewhat expected since BRA concentration is the major factor of color change. The ΔE* value of S/ES-BRA0.5 film (16.67) increased by 8.21 relative to the E* value of S/ES-BRA0 film (8.46).

One of the desired characteristics of a packaging film is that it should protect food from the effects of light, especially UV radiation (Ashrafi et al., 2018). The opacity of S/ES-BRA films was shown in Fig. 3. With the addition of BRA, the opacity of S/ES-BRA0.1 film (3.63 $Abs_{350} \cdot mm^{-1}$) was lower than the one of S/ES-BRA0 film (4.11 $Abs_{350} \cdot mm^{-1}$). The opacity of S/ES-BRA film gradually increased as the concentration of BRA increasing and the opacity of S/ES-BRA0.5 film at 350 nm (4.44 $Abs_{350} \cdot mm^{-1}$) exceeded the opacity of S/ES-BRA0 film at 350 nm. The results showed that the addition of BRA increased the opacity of S/ES-BRA film, especially the opacity under UV light (350–400 nm), and the S/ES-BRA films had stronger opacity under UV light than under visible light, which might attribute to the color of S/ES-BRA film.

3.3. Mechanical properties of S/ES-BRA films

The mechanical properties of S/ES-BRA films are shown Fig. 4. Elongation at break refers to the maximum degree of elongation a

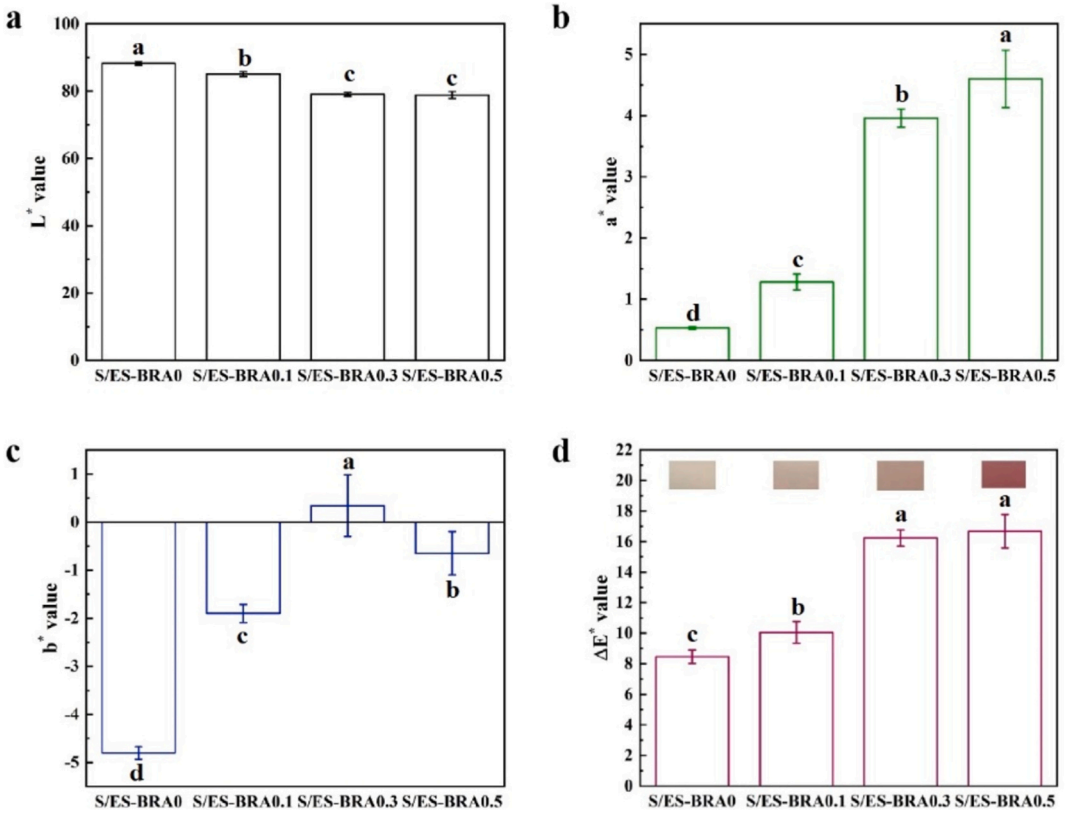

Fig. 2. The color parameters of S/ES-BRA films: (a) L* value, (b) a* value, (c) b* value, (d) total color difference (ΔE*) and appearance.

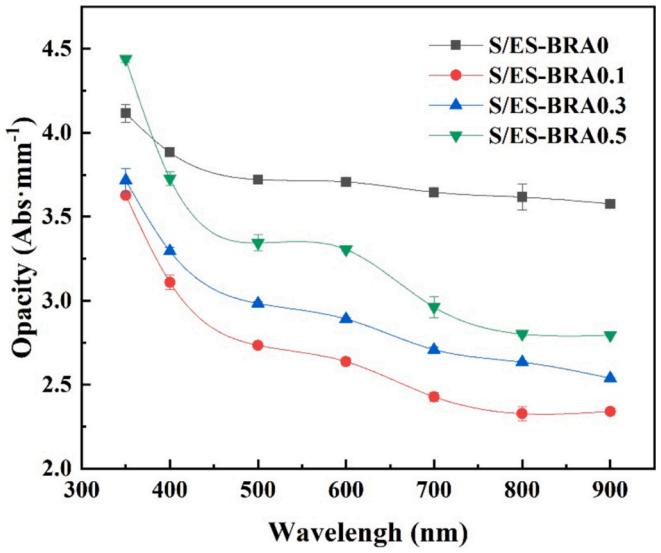

Fig. 3. UV–visible spectra of S/ES-BRA films.

material can withstand before breaking and is usually expressed as a percentage, which indicates the flexibility of S/ES-BRA films. Tensile strength refers to the maximum tensile stress sustained by the sample during the tension test, which indicates the strength of S/ES-BRA films. The S/ES-BRA films were relatively soft and flexible. The elongation at break of S/ES-BRA0 film was 33.1 %, the tensile strength was 7.3 MPa and the Young's modulus was 24.1 MPa. As the concentration of BRA increasing, the elongation at break of S/ES-BRA films increased and the tensile stress of S/ES-BRA films decreased. Compared with S/ES-BRA0 film, the elongation at break of S/ES-BRA0.5 film increased from 33.1 % to 45.4 %, and the tensile strength of S/ES-BRA0.5 film decreased from 7.3 to 5.8 MPa. Consequently, the Young's modulus of S/ES-BRA film0.5 decreased from 24.1 to 12.8 MPa, which was reduced by nearly half relative to S/ES-BRA0 film. By adding BRA, the strength and stiffness of S/ES-BRA film decreased, and the flexibility increased. This may be attributed to the increased interfacial force between the BA and the polymer matrix through hydrogen bonds formation (Alizadeh-Sani et al., 2021).

3.4. Physicochemical properties of S/ES-BRA films

XRD measurements were performed to check the change in crystallinity of S/ES-BRA films as the films were formed. The XRD spectra of S/ES-BRA films and the ingredients of the films are shown in Fig. 5.

The first type of starch (A) generates obvious diffraction peaks at around 2θ of 15°and 23° with an unresolved doublet at about 2θ of 17° and 18° (Jiang et al., 2020). The result indicated that both S and ES exhibited typical A-type diffraction patterns with strong peaks at 15.1, 17.1, 18.0, and 23.0° (2θ). BRA without obvious crystalline peaks were mainly present in the amorphous state.

The relative crystallinities (RC) of ES (18.83 %) increased significantly compared to the RC of S (14.34 %), which was in agreement with previous publications (Qiu et al., 2013). There was no difference between the diffraction peaks of 0.1 %, 0.3 % and 0.5 % S/ES-BRA films, indicating that BRA was evenly dispersed in the blend film solution.

All S/ES-BRA films exhibited similar XRD patterns with changes depending on the concentration of BRA. The diffraction peaks of S, ES and BRA material were not observed in the XRD pattern of S/ES-BRA film. The intensity for diffraction peaks of S/ES-BRA films were weakened, with peaks at 16.9, 19.6, 21.8° (2θ). The RC of S/ES-BRA film slightly decreased as the concentration of BRA increasing, which suggested that the addition of BRA reduced the crystallinity of S/ES-BRA film. Compared to the RC of S/ES-BRA0 film (9.67 %), the RC of S/ES-BRA0.1 decreased to 9.17 %, the RC of S/ES-BRA0.3 decreased to

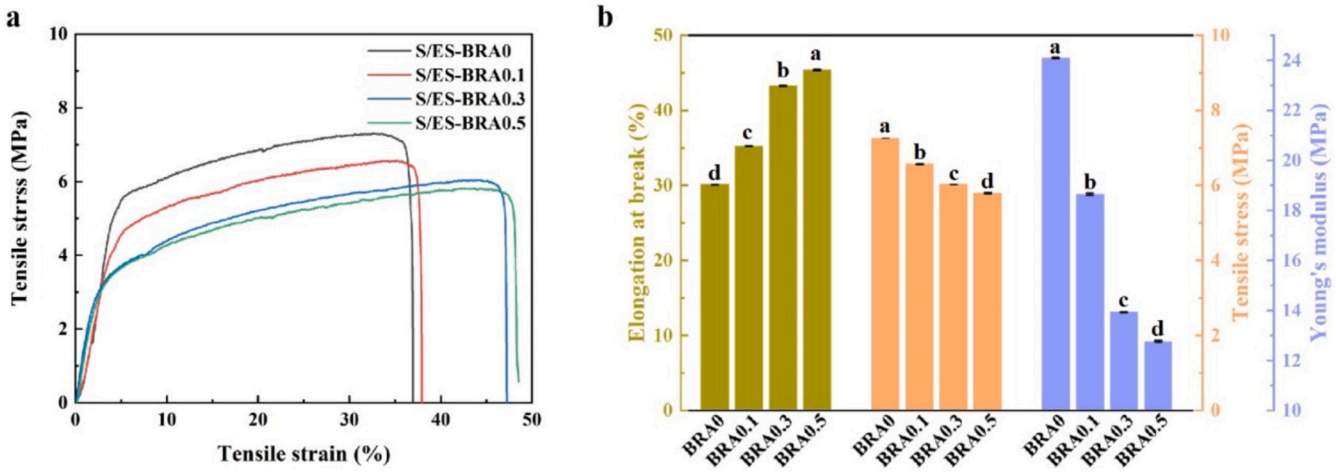

Fig. 4. (a) The tensile stress-strain curves of S/ES-BRA films; (b) elongation at break, tensile stress and Young's modulus of S/ES-BRA films.

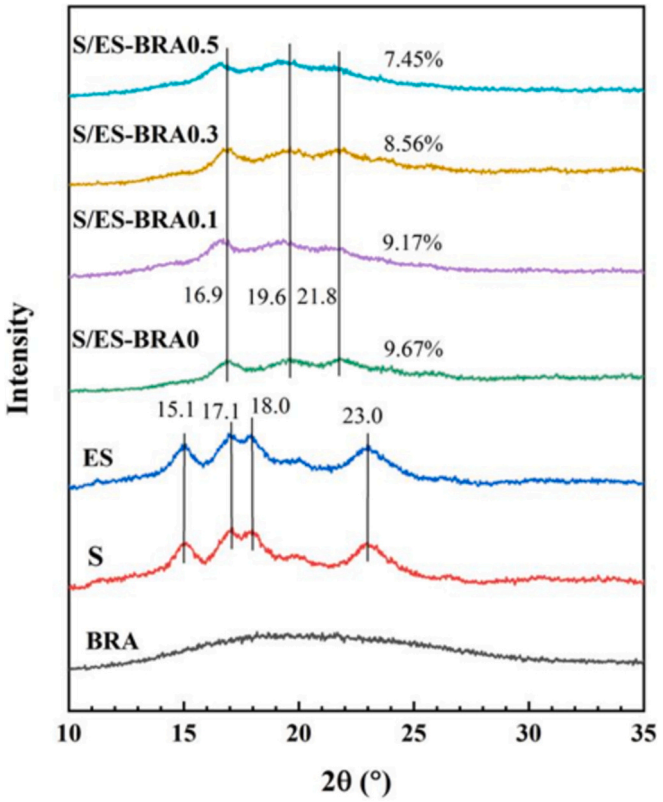

Fig. 5. X-ray diffraction patterns of S, ES, BRA and S/ES-BRA films.

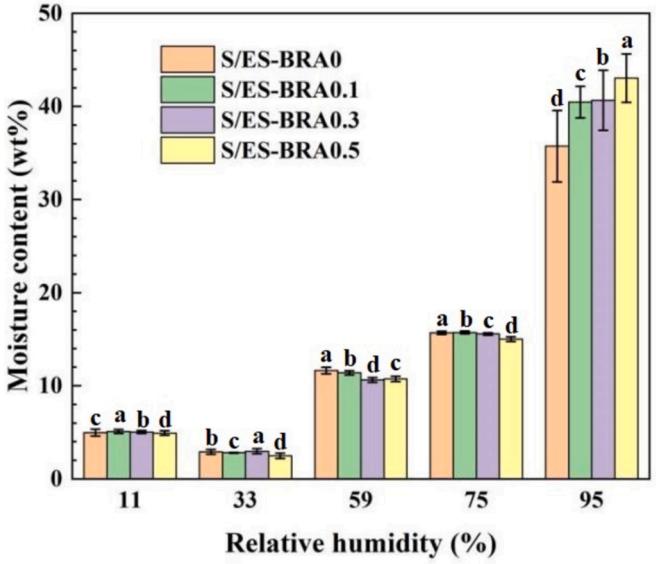

Fig. 6. Moisture absorption of S/ES-BRA films.

8.56 % and the RC of S/ES-BRA0.5 decreased to 7.45 %. The results of the crystallinity of S/ES-BRA films were consistent with the results of the tensile strength which decreased as the concentration of BRA in the film increased.

3.5. WVP of S/ES-BRA films

WVP is an essential indicator to determine the potential of water permeability of packaging films. The WVP of S/ES-BRA films was shown in Table 1. With the addition of BRA, the WVP of S/ES-BRA film increased. The WVP of S/ES-BRA0 film was 2.01 × 10–10 $g{\cdot}m^{-1}{\cdot}s^{-1}{\cdot}Pa^{-1}$ which slightly increased to 2.17 × 10–10 $g{\cdot}m^{-1}{\cdot}s^{-1}{\cdot}Pa^{-1}$ for S/ES-BRA0.1 film. The WVP of S/ES-BRA0.3 film was 2.47 × 10–10 $g{\cdot}m^{-1}{\cdot}s^{-1}{\cdot}Pa^{-1}$, which was close to 2.48 × 10–10 $g{\cdot}m^{-1}{\cdot}s^{-1}{\cdot}Pa^{-1}$, the WVP of S/ES-BRA0.5 film. Compared with the WVP of S/ES-BRA0 film, the WVP of S/ES-BRA0.5 film increased by 23.38 %. The hydrogen bonds formed between S, ES, BRA and glycerin, and the incorporation of BRA resulted in compact inner structure (it refers to a uniform, smooth cross-section structure that does not show phase separation), which is beneficial to improve the water vapor barrier property of the films (Qin et al., 2020). However, BRA increased the WVP of S/ES-BRA films, which was attributed to the hydrophilic property of BRA. Moreover, too many anthocyanin molecules formed a molecular physical space structure with larger voids, so the water-molecule transmission increased (Zhang, Sun, et al., 2020).

3.6. Water absorption of S/ES-BRA films

Water absorption indicates the water absorption ability of S/ES-BRA film when the film is immersed in water. There is no direct quantitative relationship between water absorption and solubility; the measured absorption rate indicates the degree to which the S/ES-BRA film swells during the water absorption process. The water absorption of S/ES-BRA film was shown in Table 1. S/ES-BRA0 film possessed the lowest water absorption (210.41 %). The addition of BRA increased the water

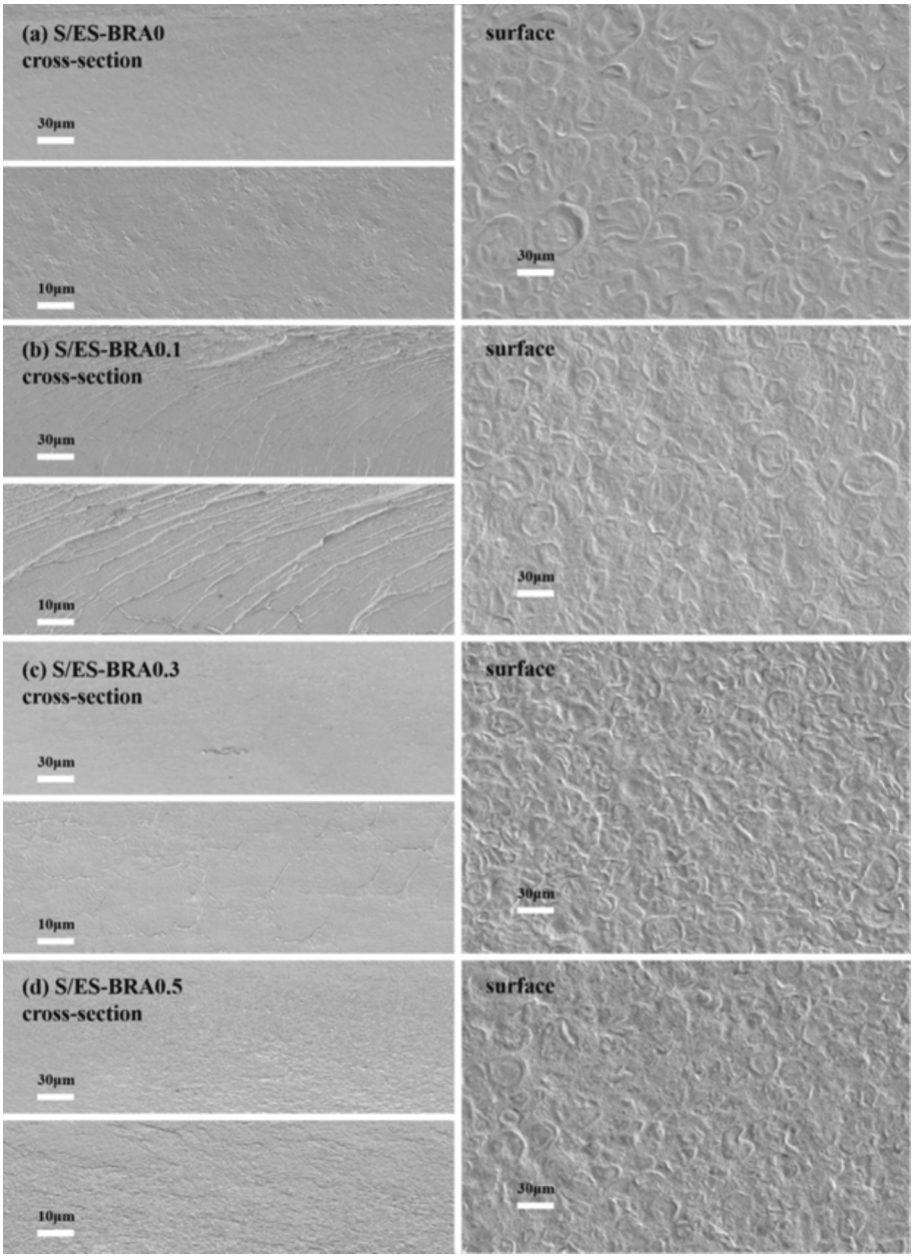

Fig. 7. The microstructure of cross-section and surface of S/ES-BRA films.

absorption of S/ES-BRA film, and S/ES-BRA0.3 film showed the highest water absorption (247.54 %). Although the water absorption of S/ES-BRA0.5 film (245.51 %) was lower than the water absorption of S/ES-BRA0.3 film, their values were very close. In general, higher water absorption is not desired for packaging due to its limitation on aqueous food (Zhang, Huang, et al., 2020). In this study, because of the hydrophilic property of S, ES, BRA and glycerin, the water absorption of S/ES-BRA film was strong and the addition of BRA increased the water absorption of S/ES-BRA film. The trend of the change of water absorption of S/ES-BRA film was similar with the WVP of S/ES-BRA film.

3.7. Moisture absorption of S/ES-BRA films

Moisture absorption indicates the ability of a material to absorb moisture in the air. The moisture absorption of S/ES-BRA film is shown in Fig. 6. In terms of humidity, for example, different ambient humidity levels have an impact on the performance of the film. Hygroscopic properties of the film at five different humidity levels. The S/ES-BRA films at 33 % RH had the lowest moisture content (2.7 wt% on average), and the S/ES-BRA films at 95 % RH had the highest moisture content (39.4 wt% on average). The difference of moisture content between S/ES-BRA films at 33 % RH and 95 % RH was about 36.7 wt%. When S/ES-BRA films were at 95 % RH, the moisture content of S/ES-BRA film increased as the concentration of BRA increased due to the hydrophilic property of S, ES, BRA and glycerin. This was because starch, glycerol and anthocyanins contained hydrophilic hydroxyl groups, which had better moisture absorption under higher humidity. However, the moisture content of S/ES-BRA films at other RH had no obvious difference. Moreover, at 95 % RH, the moisture content of S/ES-BRA0.1 film and the moisture content of S/ES-BRA0.3 film were close, which could be related to the electrostatic interactions and hydrogen bonding between S, ES and BRA (Cheng et al., 2022).

3.8. Morphology of S/ES-BRA films

The microstructure of the cross-section surface of S/ES-BRA films is

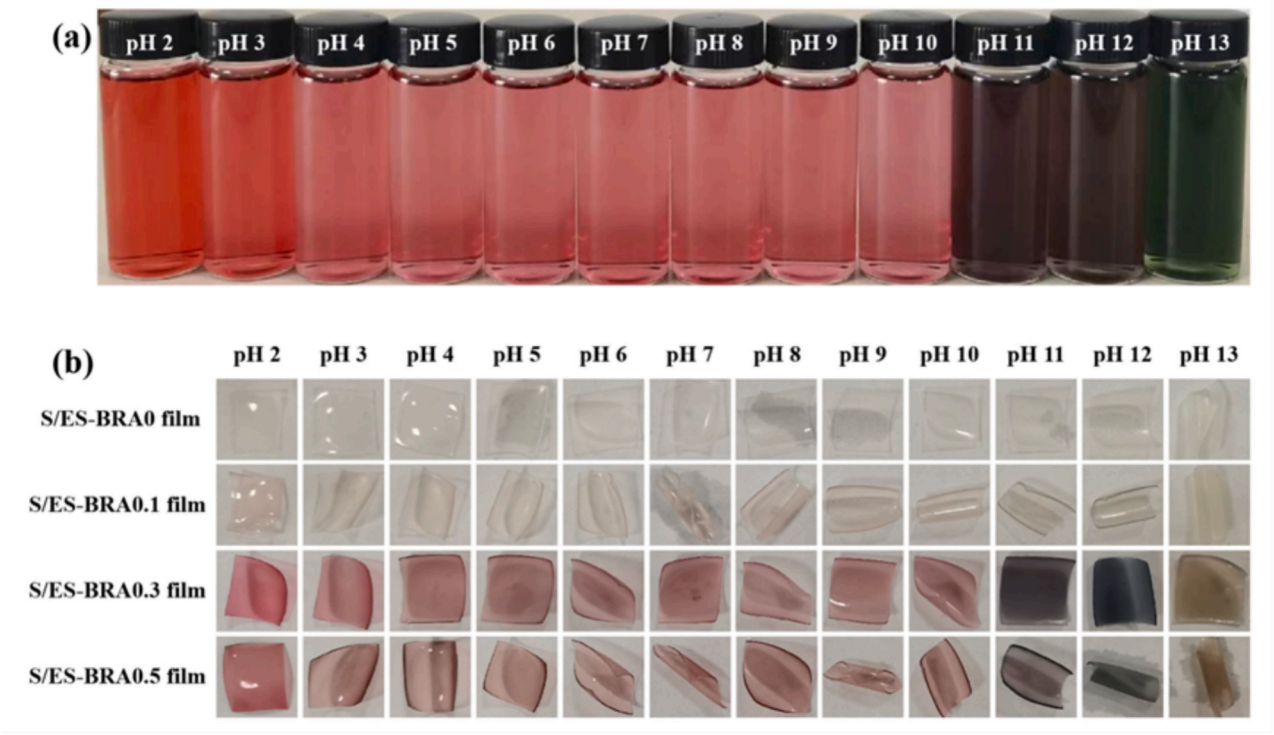

Fig. 8. (a) The color changes of BRA in different buffer solutions; (b) the pH-respond of S/ES-BRA films.

shown in the Fig. 7. The cross-section of S/ES-BRA0 film was before and after the addition of BRA and observed a uniform, compact and smooth., indicating that the mixture of starch and esterified starch had good compatibility. A slightly rough cross-section with strip texture was observed on S/ES-BRA0.1 film. When the BRA content increased to 0.3 %, the cross-section of S/ES-BRA0.3 film also showed a rough texture. When the content of BRA was increased to 0.5 %, the surface of S/ES-BRA0.5 film was more compact than other films. Similar to the cross section of S/ES-BRA film, the surface of the S/ES-BRA film for anthocyanin to join and become rough. The result indicated that BRA was more evenly distributed at low concentrations (0.1 wt% and 0.3 wt%), but the effect of uniformity was greater at higher concentration (0.5 wt %). Due to the higher extract content, the polymer network was disrupted (more uniform surface of films with the addition of BRA), this may be due to BRA and starch formed intermolecular hydrogen bonds, which inhibited starch retrogradation, and the structure was coarsier and less compact. This result was consistent with the results of WVP values and mechanical properties. Similarly, report about intelligent packaging films based on pH-sensitive films based on starch/polyvinyl alcohol and food anthocyanins (purple sweet potato extracts and red cabbage extracts) indicated that higher concentrations of the extract resulted in a breakdown of the polymer mesh, roughness of the cross section, higher WVP value and lower mechanical properties (Zhang, Huang, et al., 2020).

3.9. The pH response of S/ES-BRA films

Anthocyanins are plant polyphenols that are widely distributed in nature. They exist in most fruit seed coats to varying degrees. During the ripening of black rice, a large amount of anthocyanins accumulate in the seed coat, making brown rice appear red, yellow and even black (Ito & Lacerda, 2019). The color changes of BRA in different buffer solutions were shown in Fig. 8(a-b). BRA was red at pH 2–3, pink at pH 4–10, purple at pH 11–12, green at pH 13. Starch-BRA films exhibited red colors when the films were immersed in acidic solutions, which was because the structure of anthocyanins changed to flavylium cation (red)

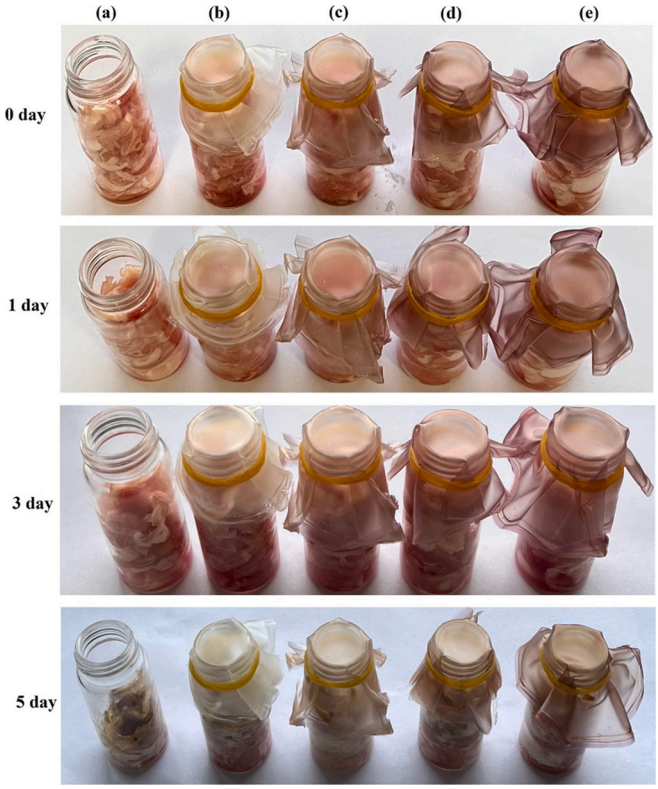

Fig. 9. Application of blank comparison (a), S/ES-BRA0 film (b), S/ES-BRA0.1 film (c), S/ES-BRA0.3 (d) and S/ES-BRA0.5 film (e).

and quinonoidal anhydrobase (purple) (Liu et al., 2017). Besides, the flavylum cation in acidic condition turning to anionic quinoidal (green) in the alkaline solutions, causing BRA to turn into green (Prietto et al., 2017; Shahid et al., 2013).

As presented in Fig. 8b, S/ES-BRA0.1, 0.3 and 0.5 films showed color change in different buffer solutions (pH 2–13). In the same pH level, with the increase of content of BRA, the color of S/ES-BRA film intensified gradually. The S/ES-BRA0 film was colorless and showed no significant color change in different buffer solutions. The color of S/ES-BRA0.1 film was relatively light. S/ES-BRA0.3 and 0.5 films had clear color change, which was similar to the color change of BRA in different buffers. The results indicated that the pH response of S/ES-BRA films was attributed to BRA.

3.10. Application of S/ES-BRA films

The number of storage days for fresh food within the shelf life is generally about 3 days even though the storage conditions vary. To ensure consumers' health and taste, it is not recommended to consume prepared dishes or foods that have gone bad (Nabi et al., 2023). In determining the film's freshness retention performance, pork not covered with any film was used as a control group to verify the film's freshness retention performance. When applied, the film does not come into direct contact with the food, but leaves a sufficiently safe reaction distance for the alkaline gases emitted by the food during the deterioration process to interact with the film.

Combined with the physical properties of S/ES-BRA films, it was easy to see that the S/ES-BRA films had the effect of preserving the freshness of pork belly in Fig. 9. The difference in pH value existed in fresh and spoiled pork belly. In general, fresh pork belly had a low pH value, whereas spoiled pork belly was provided with a relatively high pH value. This was because enzymes and bacteria decomposed the proteins and produced ammonia and amine nitrogenous substances that caused the pH value to become higher during the deterioration process of pork belly. These alkaline substances were volatile and caused the color of the S/ES-BRA films to change. As S/ES-BRA0 film had no pH–sensing ability, no obvious color change appeared during the trial of pork belly spoilage. It was important to note that the color of S/ES-BRA0.5 films changed from purple to brownish yellow as the spoilage. This suggested that S/ES-BRA0.5 films could be used as indicator films to monitor food spoilage in visual intelligent packaging.

Anthocyanins have good stability after forming a film with starch and esterified starch, the color of the film changes under pH conditions, and the color can be changed rapidly within ten seconds or so, and it is observed that no fading occurs after 24 h, which lasts for a long period of time and has a high degree of stability (Kumar et al., 2024). During molecular migration, the volatile alkaline gases in the food come into contact with the film. The film is non-toxic, even if the migration of food occurs during transport and storage, it will not have a negative impact on the human body.

4. Conclusions

The pH-sensitive composite film was successfully prepared by adding different amounts of BRA to the matrix formed by starch and esterified starch. The main components of the prepared films are corn starch, esterified starch and black rice anthocyanin, which are food-grade, non-toxic and non-polluting materials, the films can be in direct contact with food and do not pose a threat to food safety. FTIR spectra of the films showed that BRA was successfully incorporated into the starch and esterified starch matrix, resulting in a new interaction between BRA and the polymer. The addition of BRA increased the thickness, there was little variability in the density of the blend films because only a small amount of BRA was added, total color difference and cross-section of S/ES-BRA film. According to the X-ray diffraction and SEM, the addition of too much BRA made polymer grid broken and crystallinity decreased, which will lead to the physical properties of the film becoming lower and the WVP value increasing. The addition of BRA in S/ES-BRA film increased the elongation at break, water and moisture absorption of S/ES-BRA film, but reduced the tensile strength. The pH response analysis showed that the color of S/ES-BRA film changed from red to pink, to purple, and to green, as the pH value increasing. Compared with raw starch film, S/ES-BRA film is safe, non-toxic, biodegradable, and can provide a visible color response according to changes in pH, and has some toughness, so it has the potential to be used as bioactive and intelligent food packaging.

CRediT authorship contribution statement

Wei Song: Writing – original draft, Validation, Software, Investigation, Data curation, Conceptualization. **Nan Wu:** Software, Methodology, Formal analysis, Data curation. **Yikai He:** Visualization, Methodology, Data curation. **Huaixiang Zhao:** Validation, Investigation. **Jian Xu:** Validation, Funding acquisition. **Lili Ren:** Writing – review & editing, Software, Project administration, Funding acquisition.

Declaration of competing interest

The authors declare the following financial interests/personal relationships which may be considered as potential competing interests Lili Ren reports was provided by Jilin University.

Acknowledgments

This research was funded by Jilin Provincial Scientific and Technological Development Program, grant number 20230508019RC. And Graduate Innovation Fund of Jilin University, grant number 2024CX067.

Data availability

Data will be made available on request.

References

Abedi-Firoozjah, R., Yousefi, S., Heydari, M., Seyedfatehi, F., Jafarzadeh, S., Mohammadi, R., … Garavand, F. (2022). Application of red cabbage anthocyanins as pH-sensitive pigments in smart food packaging and sensors. *Polymers, 14*. https://doi.org/10.3390/polym14081629

Alizadeh-Sani, M., Tavassoli, M., Mohammadian, E., Ehsani, A., Khaniki, G. J., Priyadarshi, R., & Rhim, J.-W. (2021). pH-responsive color indicator films based on methylcellulose/chitosan nanofiber and barberry anthocyanins for real-time monitoring of meat freshness. *International Journal of Biological Macromolecules, 166*, 741–750. https://doi.org/10.1016/j.ijbiomac.2020.10.231

Amin, M. R., Anannya, F. R., Mahmud, M. A., & Raian, S. (2019). Esterification of starch in search of a biodegradable thermoplastic material. *Journal of Polymer Research, 27*. https://doi.org/10.1007/s10965-019-1983-2

Ashrafi, A., Jokar, M., & Mohammadi Nafchi, A. (2018). Preparation and characterization of biocomposite film based on chitosan and kombucha tea as active food packaging. *International Journal of Biological Macromolecules, 108*, 444–454. https://doi.org/10.1016/j.ijbiomac.2017.12.028

Bangar, S. P., Purewal, S. S., Trif, M., Maqsood, S., Kumar, M., Manjunatha, V., & Rusu, A. V. (2021). Functionality and applicability of starch-based films: An eco-friendly approach. *Foods, 10*. https://doi.org/10.3390/foods10092181

Bhargava, N., Sharanagat, V. S., Mor, R. S., & Kumar, K. (2020). Active and intelligent biodegradable packaging films using food and food waste-derived bioactive compounds: A review. *Trends in Food Science & Technology, 105*, 385–401. https://doi.org/10.1016/j.tifs.2020.09.015

Cheng, M., Yan, X., Cui, Y., Han, M., Wang, Y., Wang, J., … Wang, X. (2022). Characterization and release kinetics study of active packaging films based on modified starch and red cabbage anthocyanin extract. *Polymers, 14*. https://doi.org/10.3390/polym14061214

Choi, I., Lee, J. Y., Lacroix, M., & Han, J. (2017). Intelligent pH indicator film composed of agar/potato starch and anthocyanin extracts from purple sweet potato. *Food Chemistry, 218*, 122–128. https://doi.org/10.1016/j.foodchem.2016.09.050

Cui, C., Ji, N., Wang, Y., Xiong, L., & Sun, Q. (2021). Bioactive and intelligent starch-based films: A review. *Trends in Food Science & Technology, 116*, 854–869. https://doi.org/10.1016/j.tifs.2021.08.024

Dai, L., Zhang, J., & Cheng, F. (2019). Effects of starches from different botanical sources and modification methods on physicochemical properties of starch-based edible films. *International Journal of Biological Macromolecules, 132*, 897–905. https://doi.org/10.1016/j.ijbiomac.2019.03.197

Grobelna, A., Kalisz, S., & Kieliszek, M. (2019). Effect of processing methods and storage time on the content of bioactive compounds in blue honeysuckle berry purees [J]. *Agronomy-Basel, 9*(12).

Hasanah, N. N., Azman, E. M., Rozzamri, A., Abedin, N. H. Z., & Ismail-Fitry, M. R. (2023). A systematic review of butterfly pea flower (Clitoria ternatea L.): Extraction and application as a food freshness pH-Indicator for polymer-based intelligent packaging. *Polymers, 15*. https://doi.org/10.3390/polym15112541

Hu, X., Jia, X., Zhi, C., Jin, Z., & Miao, M. (2019). Improving properties of normal maize starch films using dual-modification: Combination treatment of debranching and hydroxypropylation. *International Journal of Biological Macromolecules, 130*, 197–202. https://doi.org/10.1016/j.ijbiomac.2019.02.144

Huang, S., Xiong, Y., Zou, Y., Dong, Q., Ding, F., Liu, X., & Li, H. (2019). A novel colorimetric indicator based on agar incorporated with Arnebia euchroma root extracts for monitoring fish freshness. *Food Hydrocolloids, 90*, 198–205. https://doi.org/10.1016/j.foodhyd.2018.12.009

Ito, V. C., & Lacerda, L. G. (2019). Black rice (Oryza sativa L.): A review of its historical aspects, chemical composition, nutritional and functional properties, and applications and processing technologies. *Food Chemistry, 301*. https://doi.org/10.1016/j.foodchem.2019.125304

Jiang, G., Hou, X., Zeng, X., Zhang, C., Wu, H., Shen, G., Li, S., Luo, Q., Li, M., Liu, X., Chen, A., Wang, Z., & Zhang, Z. (2020). Preparation and characterization of indicator films from carboxymethyl-cellulose/starch and purple sweet potato (Ipomoea batatas (L.) lam) anthocyanins for monitoring fish freshness. *International Journal of Biological Macromolecules, 143*, 359–372. https://doi.org/10.1016/j.ijbiomac.2019.12.024

Kumar, N., Pratibha, J., Prasad, J., et al. (2023). Recent trends in edible packaging for food applications - perspective for the future [J]. *Food Engineering Reviews, 15*(4), 718–747.

Kumar, N., Upadhyay, A., Shukla, S., et al. (2024). Next generation edible nanoformulations for improving post-harvest shelf-life of citrus fruits [J]. *Journal of Food Measurement and Characterization, 18*(3), 1825–1856.

Liu, B., Xu, H., Zhao, H., Liu, W., Zhao, L., & Li, Y. (2017). Preparation and characterization of intelligent starch/PVA films for simultaneous colorimetric indication and antimicrobial activity for food packaging applications. *Carbohydrate Polymers, 157*, 842–849. https://doi.org/10.1016/j.carbpol.2016.10.067

Liu, J., Zhou, H., Song, L., Yang, Z., Qiu, M., Wang, J., & Shi, S. (2021). Anthocyanins: Promising natural products with diverse pharmacological activities. *Molecules, 26*. https://doi.org/10.3390/molecules26133807

Luchese, C. L., Sperotto, N., Spada, J. C., & Tessaro, I. C. (2017). Effect of blueberry agro-industrial waste addition to corn starch-based films for the production of a pH-indicator film. *International Journal of Biological Macromolecules, 104*, 11–18. https://doi.org/10.1016/j.ijbiomac.2017.05.149

Mehboob, S., Ali, T. M., Sheikh, M., & Hasnain, A. (2020). Effects of cross linking and/or acetylation on sorghum starch and film characteristics. *International Journal of Biological Macromolecules, 155*, 786–794. https://doi.org/10.1016/j.ijbiomac.2020.03.144

Nabi, B. G., Mukhtar, K., Ahmed, W., et al. (2023). Natural pigments: Anthocyanins, carotenoids, chlorophylls, and betalains as colorants in food products [J]. Food. *Bioscience*, 52.

Prietto, L., Mirapalhete, T. C., Pinto, V. Z., Hoffmann, J. F., Vanier, N. L., Lim, L.-T., … E. d.R.. (2017). Zavareze, pH-sensitive films containing anthocyanins extracted from black bean seed coat and red cabbage, Lwt-food. *Science and Technology, 80*, 492–500. https://doi.org/10.1016/j.lwt.2017.03.006

Qin, Y., Liu, Y., Zhang, X., & Liu, J. (2020). Development of active and intelligent packaging by incorporating betalains from red pitaya (Hylocereus polyrhizus) peel into starch/polyvinyl alcohol films. *Food Hydrocolloids, 100*. https://doi.org/10.1016/j.foodhyd.2019.105410

Qiu, L., Hu, F., & Peng, Y. (2013). Structural and mechanical characteristics of film using modified corn starch by the same two chemical processes used in different sequences. *Carbohydrate Polymers, 91*, 590–596. https://doi.org/10.1016/j.carbpol.2012.08.072

Ren, L., Yan, X., Zhou, J., Tong, J., & Su, X. (2017). Influence of chitosan concentration on mechanical and barrier properties of corn starch/chitosan films. *International Journal of Biological Macromolecules, 105*, 1636–1643. https://doi.org/10.1016/j.ijbiomac.2017.02.008

Shahid, M., Shahid ul, I., & Mohammad, F. (2013). Recent advancements in natural dye applications: A review. *Journal of Cleaner Production, 53*, 310–331. https://doi.org/10.1016/j.jclepro.2013.03.031

Shernbagam, A., Kumar, N., Rahul, K., et al. (2023). Characterization of aloe Vera gel-based edible coating with Orange Peel essential oil and its preservation effects on button mushroom (Agaricus bisporus) [J]. *Food and Bioprocess Technology, 16*(12), 2877–2897.

Thakur, R., Pristijono, P., Scarlett, C. J., Bowyer, M., Singh, S. P., & Vuong, Q. V. (2019). Starch-based films: Major factors affecting their properties. *International Journal of Biological Macromolecules, 132*, 1079–1089. https://doi.org/10.1016/j.ijbiomac.2019.03.190

Vedove, T. M. A. R. D., Maniglia, B. C., & Tadini, C. C. (2021). Production of sustainable smart packaging based on cassava starch and anthocyanin by an extrusion process. *Journal of Food Engineering, 289*. https://doi.org/10.1016/j.jfoodeng.2020.110274

Xu, H., Cheng, H., McClements, D. J., Chen, L., Long, J., & Jin, Z. (2022). Enhancing the physicochemical properties and functional performance of starch-based films using inorganic carbon materials: A review. *Carbohydrate Polymers, 295*. https://doi.org/10.1016/j.carbpol.2022.119743

Zeng, F., Ye, Y., Liu, J., & Fei, P. (2023). Intelligent pH indicator composite film based on pectin/chitosan incorporated with black rice anthocyanins for meat freshness monitoring. *Food Chemistry: X, 17*. https://doi.org/10.1016/j.fochx.2022.100531

Zhang, C., Sun, G., Cao, L., & Wang, L. (2020). Accurately intelligent film made from sodium carboxymethyl starch/kappa-carrageenan reinforced by mulberry anthocyanins as an indicator. *Food Hydrocolloids, 108*. https://doi.org/10.1016/j.foodhyd.2020.106012

Zhang, K., Huang, T.-S., Yan, H., Hu, X., & Ren, T. (2020). Novel pH-sensitive films based on starch/polyvinyl alcohol and food anthocyanins as a visual indicator of shrimp deterioration. *International Journal of Biological Macromolecules, 145*, 768–776. https://doi.org/10.1016/j.ijbiomac.2019.12.159